

Photoassociation with chirped laser pulses: calculation of the absolute number of molecules per pulse

Christiane P Koch^{1,2}, Ronnie Kosloff¹, Eliane Luc-Koenig³,
Françoise Masnou-Seeuws³ and Anne Crubellier³

¹ Department of Physical Chemistry and The Fritz Haber Center, The Hebrew University, Jerusalem 91904, Israel

² Freie Universität Berlin, Fachbereich Physik, Arnimallee 14, 14195 Berlin, Germany

³ Laboratoire Aimé Cotton, CNRS, bâtiment 505, Campus d'Orsay, 91405 Orsay Cedex, France

E-mail: ckoch@physik.fu-berlin.de

Received 5 June 2006, in final form 6 August 2006

Published 25 September 2006

Online at stacks.iop.org/JPhysB/39/S1017

Abstract

The total number of molecules produced in a pulsed photoassociation of ultracold atoms is a crucial link between theory and experiment. A calculation based on first principles can determine the experimental feasibility of a pulsed photoassociation scheme. The calculation method considers an initial thermal ensemble of atoms. This ensemble is first decomposed into a representation of partial spherical waves. The photoassociation dynamics is calculated by solving the multichannel time-dependent Schrödinger equation on a mapped grid. The molecules are primarily assembled in a finite region of internuclear distances, the 'photoassociation window'. The ensemble average was calculated by adding the contributions from initial scattering states confined to a finite volume. These states are Boltzmann averaged where the partition function is summed numerically. Convergence is obtained for a sufficiently large volume. The results are compared to a thermal averaging procedure based on scaling laws which leads to a single representative initial partial wave which is sufficient to represent the density in the 'photoassociation window'. For completeness a third high-temperature thermal averaging procedure is described which is based on random phase thermal Gaussian initial states. The absolute number of molecules in the two first calculation methods agree to within experimental error for photoassociation with picosecond pulses for a thermal ensemble of rubidium or caesium atoms in ultracold conditions.

(Some figures in this article are in colour only in the electronic version)

1. Introduction

The challenge to achieve a large number of stable ultracold molecules in a trap is the prerequisite for ultracold chemistry (Doyle *et al* 2004). A good starting point is an ensemble of ultracold atoms, where photoassociation has been proven to be an efficient method to form diatomic molecules from a pair of atoms (Weiner *et al* 1999, Masnou-Seeuws and Pillet 2001). Those ultracold molecules are in a short-lived electronically excited state: in order to obtain long-lived molecules in the singlet ground or lowest triplet state, a stabilization step has to follow. The initial experiments used continuous-wave (cw) lasers, and the stabilization of the photoassociated molecule was achieved by spontaneous emission (Fioretti *et al* 1998). As a result the overall process is non-unitary and leads to an ensemble of molecules distributed over many vibrational states. The stabilization step can also be implemented within a two-colour experiment. However, with cw lasers the two-colour scheme is fully time reversible, i.e. molecules are both associated and dissociated. By employing a sequence of short laser pulses, the time-reversal symmetry can be overcome leading to a unitary process.

Moreover, together with short pulses, the concepts of coherent control can be introduced to optimize the molecule formation process. Photoassociation with chirped picosecond pulses was considered theoretically by Vala *et al* (2000) and Luc-Koenig *et al* (2004a, 2004b). Due to the finite bandwidth of short laser pulses, the resonance condition is fulfilled for a finite region of internuclear distances, the ‘*photoassociation window*’. Chirping the pulse moves the instantaneous laser frequency $\nu(t)$ through the spectral bandwidth of the pulse. Correspondingly, the distance $R_C(t)$ characteristic of the photoassociation resonance is modified, and sweeps the photoassociation window. The parameters of the pulse can be chosen to realize a molecular π -pulse and to fulfil adiabatic transfer conditions (Vala *et al* 2000, Luc-Koenig *et al* 2004a). These dynamics can be interpreted as complete transfer of the population from the ground to the excited state within the photoassociation window (Luc-Koenig *et al* 2004a). The photoassociation rate is then fully determined by the initial population within this window. Furthermore, with chirped picosecond pulses it is possible to create shaped vibrational wavepackets in the electronically excited state of a molecule such as Cs_2 (Luc-Koenig *et al* 2004a, 2004b). The shaping of these wavepackets may be optimized for radiative stabilization with a second pulse into low vibrational levels of the ground state. Such an optimization of two-colour experiments was recently discussed by Koch *et al* (2006a, 2006b).

However, at present there is no experimental evidence that photoassociation with femto- or picosecond pulses are efficient in forming ground state molecules. In conditions where photoassociation with cw lasers was successfully demonstrated, two experiments employing short pulses resulted only in the dissociation of molecules already present in the trap. This dissociation could be controlled using feedback control (Salzmann *et al* 2006) and chirped laser pulses (Brown *et al* 2006). These findings indicate that in those experiments the dissociation rate was larger than the association rate. In order to estimate the feasibility of ground state molecule formation with pulsed lasers, and to suggest possible improvements for the experimental schemes, it is crucial to calculate the absolute number of molecules.

Such a calculation necessitates quantum simulation based on first principles. A correct description of the initial scattering state is required. Two different methods are employed: (i) at higher temperatures, far from threshold, random phase thermal wavepackets may be used (Gelman and Kosloff 2003) which become Gaussian when only kinetic energy is considered (Vardi *et al* 1997, 2000). (ii) In the ultracold regime, stationary collision states which faithfully represent quantum threshold behaviour need to be employed to represent the initial state (Machholm *et al* 1994, Luc-Koenig *et al* 2004b). Quantum threshold effects appear when the

de Broglie wavelength becomes large compared to the scale of the interatomic potential and cannot be described in the framework of a semiclassical model (Julienne and Mies 1989, Julienne *et al* 1993, Julienne 1996, Weiner *et al* 1999). For the case of *s*-wave scattering, the threshold effects manifested in the photoassociation of ultracold alkali atoms have been systematically investigated by introducing the simplest asymptotic model to describe the ground molecular state (Crubellier and Luc-Koenig 2006). Marked departures from the Wigner threshold law are manifested, but scaling laws can still be derived.

With both choices for the initial state, an averaging procedure needs to be employed to calculate expectation values for the thermal ensemble of ultracold atoms. Using method (ii) it seems at first sight that cumbersome calculations on a large sample of initial collision states are necessary to perform the thermal average. However, the existence of scaling laws allow for a significant reduction of the numerical effort. In the case discussed above, adiabatic population transfer from the ground to the excited state is restricted to the region of the ‘*photoassociation window*’. For large enough detuning, this window is located in a region of relatively short internuclear distances where the nodal structure of the initial wavefunction is basically energy independent for the range of collision energies which play a role in the thermal average. The dynamics therefore remains qualitatively the same in this energy range. The energy dependence of the photoassociation probability is described by a scaling factor, determined from a short-range physical quantity such as an appropriate Franck–Condon factor. Simulating the dynamics for only one initial collision energy combined with the knowledge of the thermal probability density is then enough to estimate the thermal expectation value. This is known in statistical mechanics as the ‘maximum term method’ (Hill 1960). It was used in previous work (Luc-Koenig *et al* 2004b) to estimate the photoassociation yield, assuming that only *s* waves contribute. However, contribution of other partial waves may have to be considered. Moreover, this estimate relies upon the validity of the photoassociation window concept, while the pulse may transfer population to the excited state by different mechanisms. The scaling procedure is then no longer adapted.

The aim of the present paper is to check the validity of the scaling procedure, under conditions where it is expected to be applicable, by a general method for calculating thermal expectation values in grid-based simulations. It is based on a decomposition into partial spherical waves, i.e. the contribution of higher partial waves can be easily evaluated. The paper is organized as follows: section 2 describes the different methods available to calculate thermal averages and hence expectation values at finite temperature. The model of photoassociation with chirped laser pulses is recalled in section 3 and specified for the examples of rubidium and caesium. The convergence of the general averaging procedure is demonstrated in section 4, while section 5 introduces a simplified method due to a scaling law near quantum threshold. The total photoassociation probability is calculated in section 6 with both the general procedure and using the scaling law. Section 7 tackles the generalization to situations where the concept of the photoassociation window is no longer valid. Conclusions, in particular with respect to the feasibility of short pulse photoassociation experiments are drawn in section 8.

2. Methods to calculate the photoassociation probability in a sample of atoms in thermal equilibrium

A thermal ensemble of ground state cold atoms with binary collisions governed by one potential V_g is considered. Photoassociation with a laser pulse is transferring population into an excited electronic state with potential V_e .

2.1. Thermal averages on a finite-size grid

In grid-based methods, operators and wavefunctions are represented at a finite number of coordinate-space points which cover a limited spatial range. The basic idea in the following considerations is to connect the volume corresponding to the grid (the ‘box’) on which the Hamiltonian is represented to the physical volume of interest, such as the trapping volume of a magneto-optical trap (MOT). The underlying assumption is that the physical process of interest occurs in a finite region of space which can be modelled by the box. It is the goal of the present study to determine the total photoassociation probability per pulse $P(T)$ which is calculated as the expectation value of the projector onto the electronically excited state(s), $\hat{\mathbf{P}}_e$, at a time t_f when the photoassociation pulse is over. However, the following considerations are general and hold for other observables as well.

For a gas of N atoms confined in a volume V at temperature T , the thermally averaged expectation value of $\hat{\mathbf{P}}_e$ is defined as

$$\begin{aligned} P(T) &= \langle \hat{\mathbf{P}}_e \rangle_T = \text{Tr}[\hat{\mathbf{P}}_e \hat{\rho}_T(t_f)] \\ &= \text{Tr}[\hat{\mathbf{P}}_e \hat{\mathbf{U}}^\dagger(t_f, t_0) \hat{\rho}_T(t_0) \hat{\mathbf{U}}(t_f, t_0)]. \end{aligned} \quad (1)$$

$\hat{\mathbf{U}}(t_f, t_0)$ denotes the time-evolution operator which includes the interaction with the photoassociation laser and $\hat{\rho}_T(t_0)$ the initial density operator. Assuming that the system is in thermal equilibrium before the pulse acts, $\hat{\rho}_T(t_0)$ is given by

$$\hat{\rho}_T(t_0) = \frac{1}{Z_{\text{eq}}} e^{-\beta \hat{\mathbf{H}}}, \quad (2)$$

where $\beta = 1/(k_B T)$ (k_B the Boltzmann constant), $Z_{\text{eq}} = \text{Tr}[e^{-\beta \hat{\mathbf{H}}}]$ the partition function and $\hat{\mathbf{H}}$ the Hamiltonian.

The Hamiltonian is represented on a finite grid in coordinate space. This corresponds to dividing the physical volume V into M small boxes of volume v_{box} with the assumption that $M \geq N$. This assumption is justified because of the diluteness of the gas. The probability of finding one atom in the small box is then given by

$$P_{1,\text{box}} = \frac{N}{M} = N \frac{v_{\text{box}}}{V}, \quad (3)$$

and the probability of finding two atoms in the small box is

$$P_{2,\text{box}} = N \frac{v_{\text{box}}}{V} \cdot (N-1) \frac{v_{\text{box}}}{V} \approx N^2 \frac{v_{\text{box}}^2}{V^2} = P_{1,\text{box}}^2.$$

The total number of excited state molecules is obtained as

$$\begin{aligned} N_{\text{exc,tot}}^{\text{mol}} &= \frac{1}{2} N_e^{\text{atom}} = \frac{1}{2} M P_{1,\text{box}}^2 \langle \hat{\mathbf{P}}_e \rangle_{T,\text{box}} \\ &= \frac{1}{2} N^2 \frac{v_{\text{box}}}{V} \langle \hat{\mathbf{P}}_e \rangle_{T,\text{box}}. \end{aligned} \quad (4)$$

$\langle \hat{\mathbf{P}}_e \rangle_{T,\text{box}}$ is calculated in the two-atom picture. Three-body and higher order effects may be neglected, due to the diluteness of the gas. Centre of mass and internuclear degrees of freedom of the two-atom system are assumed to be decoupled which holds for homogeneous systems and for harmonic traps. The operators $\hat{\mathbf{P}}_e$ and $\hat{\mathbf{U}}(t_f, t_0)$ act only in the subspace of internuclear motion. The partition function factorizes for uncoupled degrees of freedom such that the centre-of-mass parts are eliminated in the thermal average. Therefore, $\langle \hat{\mathbf{P}}_e \rangle_{T,\text{box}}$ is calculated in the internuclear degrees of freedom,

$$\langle \hat{\mathbf{P}}_e \rangle_{T,\text{box}} = \frac{1}{Z_{\text{eq,box}}} \sum_{nlm} \langle \varphi_{nlm} | \hat{\mathbf{U}}^\dagger(t_f, t_0) \hat{\mathbf{P}}_e \hat{\mathbf{U}}(t_f, t_0) e^{-\beta \hat{\mathbf{H}}_g} | \varphi_{nlm} \rangle, \quad (5)$$

where $|\varphi_{nlm}\rangle$ are suitable orthonormal basis functions for the different degrees of freedom. Such functions depend upon the size of the box, and $Z_{\text{eq,box}}$ represents the partition function for this box,

$$Z_{\text{eq,box}} = \sum_{nlm} \langle \varphi_{nlm} | e^{-\beta \hat{\mathbf{H}}_g} | \varphi_{nlm} \rangle. \quad (6)$$

Equations (5) and (6) assume that in thermal equilibrium all atoms are initially in their electronic ground state. So far no choice of basis functions has been specified. An obvious choice allowing for the straightforward evaluation of the term $e^{-\beta \hat{\mathbf{H}}_g}$ is to take $|\varphi_{nlm}\rangle$ to be the eigenfunctions of the Hamiltonian $\hat{\mathbf{H}}_g$,

$$\hat{\mathbf{H}}_g = \hat{\mathbf{T}} + V_g(\hat{\mathbf{R}}) + \hbar^2 l(l+1)/2\mu \hat{\mathbf{R}}^2, \quad (7)$$

where μ is the reduced mass, and n, l, m label translational, rotational and magnetic quantum numbers in the standard way. The degeneracy relative to m is not lifted by $\hat{\mathbf{H}}_g$ and the sum over m can be evaluated leading to the degeneracy factor $(2l+1)/(4\pi)$. The eigenfunctions are now written $|\varphi_{nl}\rangle$. This is well adapted to the continuum levels of the ground molecular state of the alkali dimers. In such states the rotation is decoupled from the other angular momenta, provided one may neglect higher order relativistic effects such as second-order spin-orbit and spin-spin effects. This assumption is generally valid, except for caesium where the second-order terms may have a small effect.

The eigenfunctions $|\varphi_{nl}\rangle$ are obtained by representing $\hat{\mathbf{H}}_g$ on a grid (for each l) and diagonalizing it. They constitute an orthonormal basis of the Hamiltonian in the box representation. The corresponding eigenvalues are denoted by E_{nl} . The partition function of the box is then obtained as

$$Z_{\text{eq,box}} = \frac{1}{4\pi} \sum_{nl} (2l+1) e^{-\beta E_{nl}},$$

and

$$\langle \hat{\mathbf{P}}_e \rangle_{T,\text{box}} = \frac{1}{4\pi} \frac{1}{Z_{\text{eq,box}}} \sum_{nl} (2l+1) e^{-\beta E_{nl}} \langle \varphi_{nl} | \hat{\mathbf{U}}^+(t_f, t_0) \hat{\mathbf{P}}_e \hat{\mathbf{U}}(t_f, t_0) | \varphi_{nl} \rangle.$$

Writing the projector as $\hat{\mathbf{P}}_e = |e\rangle\langle e|$, the abbreviation

$$P_e^{nl}(t_f) = |\langle e | \hat{\mathbf{U}}(t_f, t_0) | \varphi_{nl} \rangle|^2 \quad (8)$$

can be introduced. $P_e^{nl}(t_f)$ represents the population on the excited state after propagating the ground state eigenstate $|\varphi_{nl}\rangle$ from initial time t_0 to final time t_f under the action of $\hat{\mathbf{U}}(t_f, t_0)$ which includes the interaction with the laser field. The thermally averaged photoassociation probability in the box is therefore given by

$$\langle \hat{\mathbf{P}}_e \rangle_{T,\text{box}} = \frac{\sum_{nl} (2l+1) e^{-\beta E_{nl}} P_e^{nl}(t_f)}{\sum_{nl} (2l+1) e^{-\beta E_{nl}}}. \quad (9)$$

The sums over n and l are cut off by the Boltzmann weight.

It is useful to write down the expression for the thermal probability density (2) of the box as a function of R . That is the 3D thermal density is written in spherical coordinates where the angular degrees of freedom have been integrated over. It can be constructed from the eigenfunctions $|\varphi_{nl}\rangle$ and eigenvalues E_{nl} ,

$$\rho_{T,\text{box}}(R) = \frac{1}{4\pi R^2} \frac{\sum_{nl} (2l+1) e^{-\beta E_{nl}} |\varphi_{nl}(R)|^2}{\sum_{nl} (2l+1) e^{-\beta E_{nl}}}. \quad (10)$$

The factor $1/R^2$ is due to the fact that the $\varphi_{nl}(R)$ are radial wavefunctions, i.e. $\Psi(R, \theta, \phi) = \sum_{nlm} \frac{1}{R} \varphi_{nl}(R) Y_{lm}(\theta, \phi)$. The convergence with respect to the number of partial

waves l needs to be analysed in order to determine how many partial waves are effectively required in the calculation. At large R , the probability density should become a constant independent of temperature reflecting the constant probability of finding two atoms in a box at a specific separation.

The derivation so far has neglected the quantum statistics. If the bosonic (fermionic) nature of the atoms has to be taken into account, the sum over l needs to be modified such that only even (odd) l values contribute.

2.2. Thermal averages via box-independent continuum states

In the previous section, all observables can be calculated directly on the grid provided the grid is large enough to faithfully represent the physics of the problem. An alternative procedure consists in calculating box-independent continuum states, hereafter referred as ‘true’ continuum states, and approximating the integral over the infinite number of continuum states (Machholm *et al* 1994, Luc-Koenig *et al* 2004b). The two approaches are connected in the sense that the approximation of ‘true’ continuum states represents a specific choice of basis. For a large enough box, a finite number of standing waves of the ‘box’ then approximates the continuum of scattering states. Changing the sum over box states to the integral over continuum states involves the density of states, and hence the familiar normalization of the ‘true’ continuum states to unit energy is obtained (Friedrich 1998).

Assuming the temperature to be low enough such that only the s -wave contributes, the density operator describing the thermal equilibrium (2) is written in this basis as

$$\hat{\rho}_s = \frac{1}{Z_{\text{eq}}} \int_0^\infty dE e^{-\beta E} |Es\rangle \langle Es|, \quad (11)$$

where the continuum eigenstates, normalized per unit energy, are linked to the box states by $|Es\rangle \equiv \sqrt{\frac{dn}{dE_{n,l=0}}} |\varphi_{n,l=0}\rangle$. If the box is large enough, the introduction of the density of states $\frac{dn}{dE_{n,l=0}} = \frac{dn}{dE} \Big|_{E_n}$ renders the definition of such continuum states independent of the size of the box.

The partition function Z_{eq} is assumed to describe a non-degenerate gas of non-interacting (and non-correlated) atoms. It can then be calculated analytically using the properties of an ideal gas,

$$Z_{\text{eq}} = Q(T)V, \quad Q(T) = \frac{(2\pi\mu k_B T)^{3/2}}{h^3}. \quad (12)$$

Note that (11) for a given l , and in particular for $l = 0$, is one dimensional. It is equivalent to (10) only if the temperature is really low enough for solely the s -wave to contribute. In particular, in (11) the numerator is calculated in 1D but the denominator Z_{eq} is obtained in 3D. Finally, the expression for $Q(T)$ in (12) is not valid when $T \rightarrow 0$.

2.3. Thermal averages via random-phase Gaussian wavepackets

A further alternative procedure starts from the limit of infinite temperature where the density operator of one pair of atoms is constant as a function of internuclear distance. Therefore it can be written as

$$\hat{\rho}_\infty(\vec{R}, \vec{R}') = \frac{1}{V} \mathbb{1} = \frac{1}{V} \delta(\vec{R} - \vec{R}'). \quad (13)$$

In the grid representation, each grid point represents a δ -function at this point, and $\hat{\rho}_\infty(\vec{R}, \vec{R}')$ can be approximated using random phase wavefunctions (Gelman and Kosloff 2003),

$$\Psi(R; \Theta) = \frac{1}{\sqrt{K}} \sum_{j=0}^{K-1} e^{i2\pi\theta_j} \delta(R - R_j),$$

where K is the total number of sampling points R_j , and Θ is a vector of random numbers θ_j distributed between zero and one. Making use of $\delta_{jj'} = \langle e^{i2\pi(\theta_j - \theta_{j'})} \rangle$, the identity operator in (13) can be decomposed as

$$\mathbb{1} = \lim_{L \rightarrow \infty} \frac{1}{L} \sum_{k=0}^{L-1} |\Psi(R; \Theta_k)\rangle \langle \Psi(R'; \Theta_k)|,$$

where Θ_k is a particular realization of the random number set.

At finite temperature, the thermal density can be written as

$$\hat{\rho}_T = \frac{e^{-\beta\hat{H}}}{Z} = \frac{e^{-\beta\hat{H}/2}}{\sqrt{Z}} \mathbb{1} \frac{e^{-\beta\hat{H}/2}}{\sqrt{Z}}.$$

This suggests a decomposition into random thermal wavefunctions defined by

$$\Psi_\beta(R; \Theta) = \frac{e^{-\beta\hat{H}/2}}{\sqrt{Z}} \Psi(R; \Theta) \quad (14)$$

such that

$$\hat{\rho}_T = \lim_{L \rightarrow \infty} \frac{1}{L} \sum_{k=0}^{L-1} |\Psi_\beta(R; \Theta_k)\rangle \langle \Psi_\beta(R'; \Theta_k)|.$$

It remains to evaluate the action of the Hamiltonian on the random phase wavefunction in (14). If the temperature is high enough such that the kinetic energy is much larger than the potential energy of the scattering states, or if the process of interest occurs at very large internuclear distances where the potential is flat, the Hamiltonian can be considered to depend only on the kinetic energy, i.e.

$$\hat{H} = \frac{\hat{p}^2}{2\mu}.$$

The thermal wavefunction therefore becomes a sum of Gaussians with random phase,

$$\Psi_\beta(R; \Theta) = \frac{1}{\sqrt{4\pi}} \frac{1}{\sqrt{Z}} \frac{2^{1/4}}{(\pi\sigma^2)^{1/4}} \frac{1}{\sqrt{K}} \sum_{j=0}^{K-1} \exp\left(-\frac{(R - R_j)^2}{4\sigma^2} + i2\pi\theta_j\right), \quad (15)$$

where the width $\sigma = \hbar\sqrt{\beta/4\mu}$ is determined by the temperature. The number K of required Gaussians is determined by the volume in which the process takes place and which needs to be sampled by the grid, for example the ‘photoassociation window’. In that case, the individual Gaussian wavefunctions inside the sum of (15) have to be used as initial states of the dynamics, and $\sum_{j=0}^{K-1}$ can be evaluated by the Monte Carlo wavefunction technique (Dalibard *et al* 1992) in order to obtain the photoassociation probability.

For $T \rightarrow 0$, the assumption that the kinetic energy dominates is not valid any longer and the full Hamiltonian would have to be employed to evaluate (14). However, in this regime the thermal wavefunction loses its meaning: since β diverges, the convergence of (14) with respect to the number of grid points K becomes extremely slow. This just reflects the fact that the thermal Gaussian wavepacket method is derived from the high-temperature limit and is not applicable at very low temperatures.

3. Model of photoassociation with chirped laser pulses and adiabatic transfer within a ‘photoassociation window’

3.1. Model of photoassociation with time-dependent laser pulses

Two ground state alkali atoms ($nS + nS$) which interact via the ground or lowest triplet state and which collide in the presence of a laser field are considered. The laser excites the pair of atoms into an electronically excited state correlated to the $nS + nP$ dissociation limit which may support bound vibrational levels. These levels give rise to the photoassociation resonances. Whereas a cw laser which is red detuned by $\Delta_L = \hbar(\omega_0 - \omega_L)$ from the frequency ω_0 of the $nS \rightarrow nP$ atomic line usually excites at resonance only a *single* vibrational level with binding energy equal to Δ_L , a laser pulse may transfer population to *several* levels within its spectral bandwidth $\hbar\delta\omega$.

A minimal model of photoassociation requires the solution of the time-dependent Schrödinger equation on two electronic states (Vala *et al* 2000, Luc-Koenig *et al* 2004a, 2004b),

$$i\hbar \frac{\partial}{\partial t} \begin{pmatrix} \bar{\psi}_e(R, t) \\ \bar{\psi}_g(R, t) \end{pmatrix} = \hat{H} \begin{pmatrix} \bar{\psi}_e(R, t) \\ \bar{\psi}_g(R, t) \end{pmatrix}, \quad (16)$$

where R denotes the internuclear distance. The Hamiltonian in the rotating-wave and dipole approximations is written as

$$\hat{H} = \begin{pmatrix} \hat{T} + V_e(\hat{\mathbf{R}}) - \hbar/2(\omega_L + \frac{d\phi}{dt}) & -\frac{1}{2}\bar{D}(R)\mathcal{E}_0 f(t) \\ -\frac{1}{2}\bar{D}(R)\mathcal{E}_0 f(t) & \hat{T} + V_g(\hat{\mathbf{R}}) + \hbar/2(\omega_L + \frac{d\phi}{dt}) \end{pmatrix}, \quad (17)$$

with $\mathcal{E}(t) = \mathcal{E}_0 f(t) \cos[\omega_L t + \phi(t)]$ being the time-dependent laser field, and $\bar{D}(R)$ the projection of the transition dipole moment onto the axis of the electric field. The rotating frame makes use of the instantaneous frequency $\frac{d}{dt}(\omega_L t + \phi(t))$, transforming a wavefunction Ψ into $\bar{\Psi}$. The dynamics of the photoassociation process is studied by numerical solution of the time-dependent Schrödinger equation (16) as described in Luc-Koenig *et al* (2004a, 2004b). The initial state of the dynamics is chosen to be a stationary scattering wavefunction of the ground state Hamiltonian. Under appropriate conditions it could also be a Gaussian wavepacket. The radial dependence of the wavepackets propagating on both surfaces is represented using mapped grid methods (Kokoouline *et al* 1999, Willner *et al* 2004). The grid step is proportional to the local de Broglie wavelength with the grid mapping parameter β_{grid} . Sine waves vanishing at the boundaries of the box are used as basis functions. The time-evolution operator $\exp[-i\hat{H}t/\hbar]$ is expanded in Chebyshev polynomials (Kosloff 1994). An extension of the model to more than two electronic states is straightforward (Koch *et al* 2006b).

Photoassociation of ^{133}Cs and ^{87}Rb will be considered. For caesium following previous work by Luc-Koenig *et al* (2004a, 2004b), and Koch *et al* (2006a), transitions from the $a^3\Sigma_u^+(6S + 6S)$ lowest triplet state into the $0_g^-(6S + 6P_{3/2})$ excited state are assumed. The $0_g^-(P_{3/2})$ potential V_e allows for efficient photoassociation due to its $1/R^3$ behaviour at large internuclear distances and for stabilization into stable molecules due to its double-well structure. Details of the potentials are found in Luc-Koenig *et al* (2004a). The transition dipole moment $\bar{D}(R)$ is taken to be independent of R . For rubidium, following Koch *et al* (2006b), the transitions into the excited states with potentials scaling at long range as $1/R^3$ below the $5S + 5P_{1/2}$ asymptote, i.e. $X^1\Sigma_g^+ \rightarrow 0_u^+(P_{1/2})$ and $a^3\Sigma_u^+ \rightarrow 1_g(P_{1/2})$, are considered. Both of these excited state potentials allow for an efficient photoassociation step,

while stabilization into stable molecules is facilitated only by $0_u^+(\text{P}_{1/2})$, but not by $1_g(\text{P}_{1/2})$. The physical mechanism of the stabilization step was identified as resonant coupling which can only be described by an explicit treatment of the spin-orbit interaction in the excited state. This leads to a three(four)-channel Hamiltonian for $0_u^+(\text{P}_{1/2})$ ($1_g(\text{P}_{1/2})$). Details of the potentials, transition dipole moments and spin-orbit interaction are found in Koch *et al* (2006b).

In the ground electronic state, the various l -waves are introduced, i.e. for $l > 0$ the rotational barrier, $\hbar^2 l(l+1)/(2\mu R^2)$, is included in $\hat{\mathbf{H}}_g$. To avoid cumbersome calculations, the rotational structure of the excited electronic state is not considered. Indeed, the transition dipole moment includes an angular part which depends on the polarization of the laser light and on the initial state of the atoms and which is different for the different rotational levels of the excited state. The relevant angular part can be evaluated in any given experimental situation, but general rules are missing.

Furthermore the Hamiltonian $\hat{\mathbf{H}}$ is spin independent. To account for the electronic spin degeneracy of the ^2S atomic state, $d_A = 2$, and of the initial electronic state, $d_{2s+1\Sigma} = 2S + 1$, while disregarding the nuclear spin, the total number of photoassociated molecules (4) has to be multiplied by the factor $d_{2s+1\Sigma}/d_A^2$.

Concerning the ground electronic state of alkali dimers, the hyperfine structure has to be included and one has to know whether the atoms are spin polarized or not. In the excited state, fine and hyperfine structures have to be taken into account since rotation is not decoupled from the other angular momenta. In the present paper, the most general part of the problem, which concerns the radial part of the wavefunctions is of interest, and the angular part of the transition dipole moment is completely ignored. It could be introduced later, specifying certain experimental conditions.

Provided that the hyperfine interaction modifies the radial wavefunctions only slightly, it is still possible to roughly account for the hyperfine structure and for the bosonic or fermionic character of the atoms by introducing convenient weights in the numerator of (9), which includes photoassociation matrix elements. If all atoms are prepared in a ‘polarized’ state with given f and m_f values, the situation of zero hyperfine coupling is recovered, i.e. for bosonic (fermionic) atoms only even (odd) l values contribute to the sum of (10). If all the atoms are prepared in a given hyperfine level, with given f value but with any m_f value, the sum has to be weighted by $(f+1)/(2f+1)$ ($f/(2f+1)$) for even (odd) l values in the case of bosonic atoms. For fermionic atoms, the same weights are respectively associated with odd (even) l values. Indeed, the excited molecular state can be only symmetric (anti-symmetric) for bosonic (fermionic) atoms, so that only symmetric (anti-symmetric) ground states play a role in photoassociation. However, the atoms of the initial state are assumed to be non-interacting, i.e. correlations are killed by decoherence effects. As a consequence, both symmetric and anti-symmetric states have to be considered in any case, both in the numerator and in the denominator of (9) and (10), and the effect of the weights becomes very small.

3.2. Photoassociation with chirped pulses and ‘photoassociation window’

A transform-limited pulse with Gaussian envelope $f(t)$, maximum at t_p and full width at half maximum of the temporal intensity profile $\tau_L = (4 \ln 2)/\delta\omega$ is considered. Chirping the pulse with a linear chirp such that $\frac{d\phi(t)}{dt} = \chi(t - t_p)$ stretches the duration to $\tau_C = F\tau_L$ with $F \geq 1$ and decreases the maximum intensity, conserving the energy carried by the pulse. Moreover 98% of this energy is carried during the *time window* $[t_p - \tau_C, t_p + \tau_C]$. For a chirped pulse, the instantaneous resonance condition varies with time as indicated in figure 1. This defines a *resonance window* with a width $2\hbar|\chi|\tau_C = 2\hbar\delta\omega\sqrt{1 - F^{-2}}$ in the

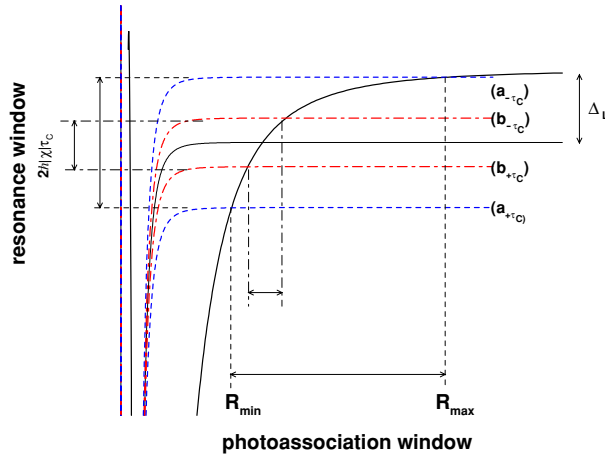


Figure 1. Scheme of the photoassociation process with two negatively chirped pulses, corresponding to the same linear chirp rate χ applied to two transform-limited (TF) pulses with duration τ_L , detuned by Δ_L with respect to the atomic resonance line. The pulses differ by their spectral bandwidth $\hbar\delta\omega \propto 1/\tau_L$ and therefore by their duration τ_C . Pulse (a) (blue curves) represents a strongly chirped pulse with a large bandwidth and long duration after chirping, pulse (b) (red curves) is a slightly chirped pulse with a narrow bandwidth and short duration after chirping τ_C . During the ‘time window’ $[-\tau_C, +\tau_C]$ the dressed ground-state potential (pulse (a): blue \cdots line, pulse (b): red $-\cdot-$ line) moves by $2\hbar\chi\tau_C$ with respect to the excited-state potential (black $—$ line). The instantaneous crossing point between the dressed potentials varies accordingly from R_{\max} to R_{\min} defining the ‘photoassociation window’ $[R_{\min}, R_{\max}]$ which is much smaller in the case of pulse (b).

energy range. The Condon point $R_C(t)$ corresponding to the instantaneous crossing of the two field-dressed potential curves moves in the spatial range $[R_{\min}, R_{\max}]$ giving rise to the concept of the ‘photoassociation window’. If the pulse parameters are appropriately chosen, adiabatic population transfer within the ‘photoassociation window’ can be achieved (Luc-Koenig *et al* 2004a). In such a regime, the photoassociation yield is governed by Franck–Condon factors even for intensities where the perturbative model is no longer valid.

4. Calculations in a 3D box: convergence of the method

Before proceeding to the calculation of the total photoassociation probability per pulse in section 6, the consistency of the method derived in section 2.1 is demonstrated. The calculation of thermal expectation values requires an averaging procedure over an ensemble of initial states, and the average is performed by simulating the photoassociation dynamics for all the initial states. The number of required simulations can be estimated by considering explicitly the thermal density operator, (2) and (10), respectively. This will be shown in section 4.1, while the convergence of thermal expectation values such as the total photoassociation probability is discussed in sections 4.2 and 4.3: thermal averages, e.g. (4), are obtained by connecting quantities which are calculated in the box such as (9) and (10), to the real physical volume. They must be independent of the box size. It will be shown below, that the R_{box} -dependence in (9) is solely due to the denominator, i.e. the normalization by $Z_{\text{eq,box}}$, and that this R_{box} -dependence cancels in the thermal average (4) due to the factor v_{box} . The weights due to the hyperfine structure are neglected in these calculations.

4.1. Initial state: 3D thermal density matrix

Since ρ_T represents an equilibrium, i.e. a static, property of the system, the hyperfine structure and the bosonic or fermionic character of the atoms need to be taken into account. However, as far as the ground state is concerned, and if the angular factor discussed in section 3.1 may be neglected, this leads just to a small modification in the sum over the rotational quantum number l in (10) provided that the hyperfine interaction only slightly modifies the radial wavefunctions. The weighting factors introduced in section 3.1 consequently appear only in the numerator of (9) and (10).

The sum over l in (9) and (10) is cut off by the Boltzmann weight. For practical calculations, it needs to be determined how many rotational states should be included. An estimate is obtained by considering the rotational Boltzmann weight,

$$w_{\text{rot}}(R) = (2l + 1) \exp(-\beta \hbar^2 l(l + 1) / 2\mu R^2),$$

at the edge of the box, $R = R_{\text{box}}$. In this work, l_{max} was fixed by demanding that $w_{\text{rot}}(R_{\text{box}}) < 0.02$ for the highest temperature considered, $T = 150 \mu\text{K}$, and the same l_{max} was used for all temperatures (implying an even better convergence with respect to l for the lower temperatures). This leads to $l_{\text{max}} = 24(30)$ for $R_{\text{box}} = 1000a_0$, $l_{\text{max}} = 135(167)$ for $R_{\text{box}} = 5000a_0$, and $l_{\text{max}} = 575(717)$ for $R_{\text{box}} = 20\,000a_0$ for ^{87}Rb (^{133}Cs). For high rotational excitation, $P_e^{nl}(t_f)$ will be small since the rotational barrier suppresses probability density of the initial state in the ‘photoassociation window’. However, large l need to be included in the calculation of the partition function to obtain converged results. This reflects the slow convergence of the expansion into spherical waves in a large box. It should also be noted that depending on temperature the largest contribution to the numerator of (9) is not necessarily obtained for s -waves but more likely for $l = 1$ or $l = 2$ due to the $(2l + 1)$ -fold degeneracy. For a given l , the maximum energy of translational states is limited by the Boltzmann factor. Since the energy of the lowest scattering state of the box decreases as $1/R_{\text{box}}^2$ and the density of states decreases as \sqrt{E}/R_{box} , the number of translational states n_{max} increases with increasing box size. Since *a priori* each combination nl corresponds to a separate simulation of the photoassociation dynamics, it is important to determine a box size which is large enough to faithfully represent the scattering states but small enough to keep $n_{\text{max}} \cdot l_{\text{max}}$ minimal. If the photoassociation occurs in the ‘photoassociation window’, the number of required simulations can be decreased in a controllable way as shown below.

In general, an estimate for the minimally required box size is obtained by considering the thermal density of the box, $\rho_{T,\text{box}}(R)$, (10), as a function of R . The box is expected to be large enough when $\rho_{T,\text{box}}(R) = \text{const}$ at large R . This is illustrated in figures 2(a) and (b) which show $\rho_{T,\text{box}}(R)$ for a pair of caesium atoms in a box of lengths $1000a_0$ and $2000a_0$. In figure 2 all partial waves l are introduced neglecting the weights due to hyperfine structure (section 3.1). The basis functions were chosen (cf section 3.1) to be sine waves in the box, because they are zero at the box boundaries (Willner *et al* 2004). This behaviour is reflected in the thermal density: since all basis functions vanish at R_{box} so does the thermal density. If the box is large enough, there is, however, a range of R values for which the thermal density is constant, and this will serve as criterion for convergence. The required box size depends on temperature: larger boxes are necessary for lower temperatures (cf black and blue lines in figure 2). This can be understood as follows: the temperature determines the range for the collision energy of the scattering states, $E_{\text{coll}} \sim k_B T$. Neglecting the modification due to the interatomic potential, the minimal collision energy of the box is simply determined by the box quantization. A thermal average for a low temperature requires the presence of a sufficient number of scattering states with very small collision energies which are present only for large boxes. For very large grids ($R_{\text{box}} \gtrsim 20\,000a_0$, data not shown), the constant value of

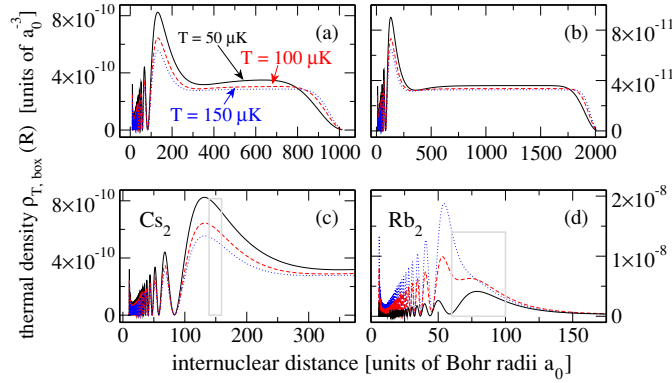


Figure 2. The thermal density (10) of two ^{133}Cs atoms (a)–(c) and of two ^{87}Rb atoms (d) as a function of R for $T = 50 \mu\text{K}$ (black solid line), $T = 100 \mu\text{K}$ (red dashed line), and $T = 150 \mu\text{K}$ (blue dotted line). ρ_T is compared for $R_{\text{box}} = 1000a_0$ and $R_{\text{box}} = 2000a_0$ in panels (a) and (b) indicating the convergence with respect to R_{box} . Panels (c) and (d) show the short-range behaviour of ρ_T for caesium and rubidium with the grey box indicating the ‘photoassociation window’ for a pulse with spectral bandwidth $\hbar\delta\omega = 0.26 \text{ cm}^{-1}$ and detuning from the atomic line $\Delta = 0.675 \text{ cm}^{-1}$ for caesium and $\hbar\delta\omega = 1.5 \text{ cm}^{-1}$ and $\Delta = 4.1 \text{ cm}^{-1}$ for rubidium. Note the different temperature dependence of the short-range part of ρ_T of rubidium as compared to caesium which is due to a shape resonance.

$\rho_T(R)$ at large R converges to the same value which depends on R_{box} but not upon the species nor on the temperature. Note that for large boxes, this constant value of $\rho_T(R)$ depends neither on the temperature nor on the studied species. In fact, this value converges to the density $1/v_{\text{box}}$ of an ideal gas confined to a volume V where each elementary volume v_{box} (cf (13)) contains only one pair of atoms.

Figures 2(c) and (d) compare the short-range part of $\rho_{T,\text{box}}$ for two ^{133}Cs atoms and for two ^{87}Rb atoms in a box of length $1000a_0$. The ‘photoassociation window’ corresponding to the two pulses used in the dynamical calculations is indicated by a grey box. It corresponds for caesium to a pulse with spectral bandwidth $\hbar\delta\omega = 0.26 \text{ cm}^{-1}$ and detuning from the atomic line $\Delta = 0.675 \text{ cm}^{-1}$ (referred to as \mathcal{P}_{-}^{122} by Koch *et al* (2006a) and for rubidium to a pulse with spectral bandwidth $\hbar\delta\omega = 1.5 \text{ cm}^{-1}$ and detuning from the atomic line $\Delta = 4.1 \text{ cm}^{-1}$ (cf Koch *et al* (2006b)). In the weak-field regime and for adiabatic population transfer, the photoassociation probability is determined, in addition to the pulse intensity, by the thermal density within the ‘photoassociation window’. The thermal density is related to $\rho_{T,\text{box}}$ analogously to (4). Note the different temperature behaviours of the probability density of rubidium compared to caesium: a shape resonance in rubidium leads to an enhancement of the probability density for $150 \mu\text{K}$ and $100 \mu\text{K}$ compared to $50 \mu\text{K}$. The largest single- l contribution to $\rho_{T,\text{box}}$ is therefore due to $l = 2$. This indicates the importance of including rotational excitations when calculating the thermal expectation value.

4.2. Convergence of the partition function: comparison with the ideal gas

The denominator of (9), the partition function of the box, $Z_{\text{eq,box}}$, is shown as a function of the box size in figure 3 and compared to the partition function of free ($V_{\text{g}}(R) \equiv 0$) spherical waves in a box and to the partition function of the ideal gas confined to the volume v_{box} (12). The eigenvalues of the free spherical waves are obtained as roots of the Bessel functions of the first kind using the numerical package RFSFNS⁴ (Vrahatis *et al* 1995). Differences between

⁴ <http://cpc.cs.qub.ac.uk/summaries/ADCK.v1.0.html>

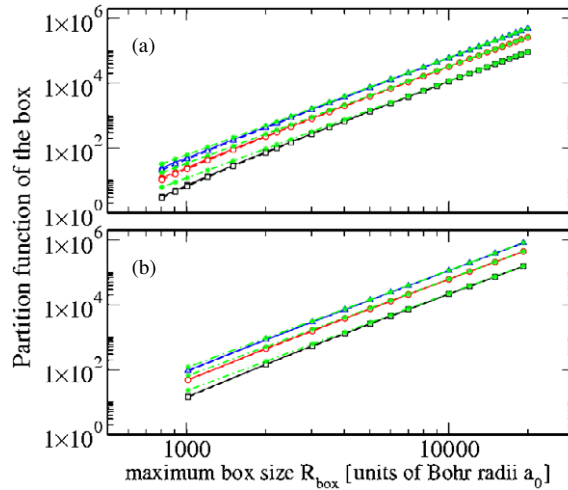


Figure 3. Partition function $Z_{\text{eq,box}}$ calculated from the eigenvalues obtained in the box as $\sum_{nl} (2l+1) e^{-\beta E_{nl}}$ (full line and filled symbols) and from the free spherical waves (i.e. the zeros of the Bessel functions, dashed lines and open symbols) as a function of the box size R_{box} for $T = 50 \mu\text{K}$ (black \square), $T = 100 \mu\text{K}$ (red \circ), and $T = 150 \mu\text{K}$ (blue \triangle). The analytical partition function for an ideal gas of non-interacting atoms (12) is also drawn for the three temperatures (green $-\cdot-$ line and stars). The log-log-scale emphasizes the scaling $Z_{\text{eq}} \sim R_{\text{box}}^3$. Shown are the values for two ^{87}Rb atoms interacting via the $X^1\Sigma_g^+$ ground state potential (a) and for two ^{133}Cs atoms interacting via the $a^3\Sigma_u^+$ potential (b).

$Z_{\text{eq,box}}$ for the true potential and for $V_g(R) \equiv 0$, where $Z_{\text{eq,box}}$ is calculated with the same l_{max} (cf section 4.1), are observed only for very small box sizes ($R \lesssim 2000a_0$). This demonstrates that the short-range part of $V_g(R)$ does not significantly modify the partition function. These values which are obtained by using a spherical wave expansion and discretization of the continuum, differ noticeably from Z_{eq} of the ideal gas for small box sizes ($R \lesssim 5000a_0$). This is explained by the minimum collisional energy of the box which is then too large and the density of states which is too small to correctly describe the thermal distribution at the studied temperatures⁵. The log-log scaling in figure 3 emphasizes the algebraic scaling of the box partition functions as $Z_{\text{eq,box}} \sim R_{\text{box}}^3$. In the calculation of the thermal average (4), this R_{box} -dependence cancels with that of the box volume v_{box} . Equivalently, for a sufficiently large box size, the factor $\frac{v_{\text{box}}}{V} \frac{1}{Z_{\text{eq,box}}}$ in (4) is identical to the factor $\frac{1}{Z_{\text{eq}}}$ in (12).

The convergence with respect to the number of partial waves l_{max} is analysed in figure 4. The partition function and the contributions to the sum are shown in figures 4(a) and (b). The convergence of the expansion in spherical waves is slow: all l up to l_{max} are required to obtain the convergence of $Z_{\text{eq,box}}$ calculated in the real potential $V_g(R)$. The same behaviour is obtained for the partition function calculated from free spherical waves in the same box (not shown). However, this slow convergence does not pose a problem since the evaluation of $Z_{\text{eq,box}}$ requires only the knowledge of the eigenvalues E_{nl} which are obtained by one matrix diagonalization (typically of dimension 1000×1000) for each l . For sufficiently large boxes ($R \gtrsim 2000a_0$), $Z_{\text{eq,box}}$ can be approximated by the partition function of the free spherical waves in a box which is obtained from the roots of the Bessel functions of the first kind requiring even less numerical effort than the matrix diagonalizations. For very

⁵ Expressed in Kelvin, the minimum collisional energy of the box varies as $19.67/R_{\text{box}}^2$ ($12.86/R_{\text{box}}^2$) for ^{87}Rb (^{133}Cs).

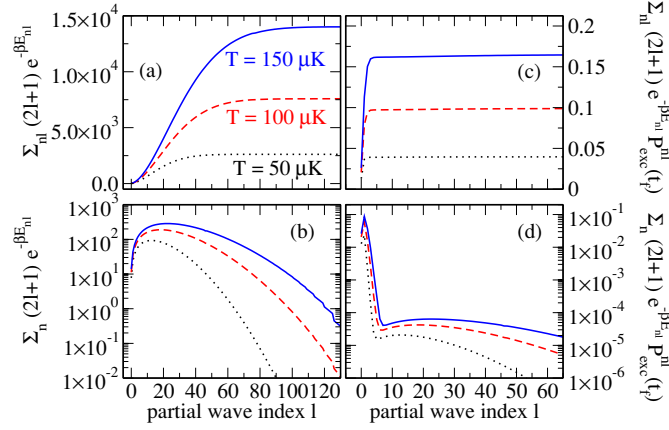


Figure 4. The partition function $\sum_{n,l'=0,l} (2l'+1) e^{-\beta E_{nl'}}$ (a), and single l' -contributions to the partition function (b), the thermal average of the excited state population $\sum_{n,l'=0,l} (2l'+1) e^{-\beta E_{nl'}} P_e^{nl'}(t_f)$ (c), and single l' -contributions to the thermal average (d), as a function of the partial wave index l for Cs($0_g^-(P_{3/2})$) and a box of length $5000a_0$ ($l_{\max} = 167$). The highest contribution to the numerator of $\langle \hat{\mathbf{P}}_e \rangle_{T,\text{box}}$ (c), (d) is due to $l' = 1$, not $l' = 0$ for all considered temperatures. The pulse is described in the text.

large boxes, $Z_{\text{eq,box}}$ becomes identical to the analytically known partition function of the ideal gas.

4.3. Convergence of the numerator in the thermally averaged photoassociation probability: potential barrier effects

Figures 4(c) and (d) present the convergence with respect to the number of partial waves of the numerator of $\langle \hat{\mathbf{P}}_e \rangle_{T,\text{box}}$ (9), i.e. of the unnormalized expectation value $Z_{\text{eq,box}} \cdot \langle \hat{\mathbf{P}}_e \rangle_{T,\text{box}}$. It is striking to see that the numerator converges very quickly with l (figure 4(a)). This rapid convergence is explained by the height of the centrifugal barrier which at low temperature suppresses collisions, and therefore photoassociation, of high- l waves. The barrier is equal to $79 \mu\text{K}$ ($35.7 \mu\text{K}$) for $l = 1$, $417 \mu\text{K}$ ($186 \mu\text{K}$) for $l = 2$, $1168 \mu\text{K}$ ($525 \mu\text{K}$) for $l = 3$ and $2513 \mu\text{K}$ ($1330 \mu\text{K}$) for $l = 4$ for ^{87}Rb (^{133}Cs). Hence the contributions to the sum in the numerator (9) shown in figure 4 quickly become very small. One can take advantage of this fact to compute (9) in a well-controlled approximation which requires much less numerical effort than the full procedure of section 2.1: the numerator, $\sum_{n,l} (2l+1) e^{-\beta E_{nl}} P_e^{nl}(t_f)$, is calculated until the desired accuracy is achieved at $l_{\text{cut}} \approx 10$ while the denominator, i.e. the partition function, is calculated with l_{\max} (or with the analytical expression for very large boxes). This reduces the numerical effort considerably since the evaluation of the numerator requires the simulation of the full dynamics while for the partition function only the ground state eigenvalues E_{nl} need to be determined.

At the considered temperatures which represent typical MOT conditions, the highest contribution to the thermal average is obtained for $l = 1$, and not for the s -wave. Even for $l = 2$, the contribution is still comparable to that of the s -wave. This corresponds to what is known from photoassociation with cw lasers: the introduction of l -waves up to $l = 4$ is necessary to interpret the 1_u photoassociation spectrum of Cs atoms in the hyperfine level $f = 3$ recorded in a dark-spot MOT at the temperature $T = 200 \mu\text{K}$ (Comparat *et al* 2000).

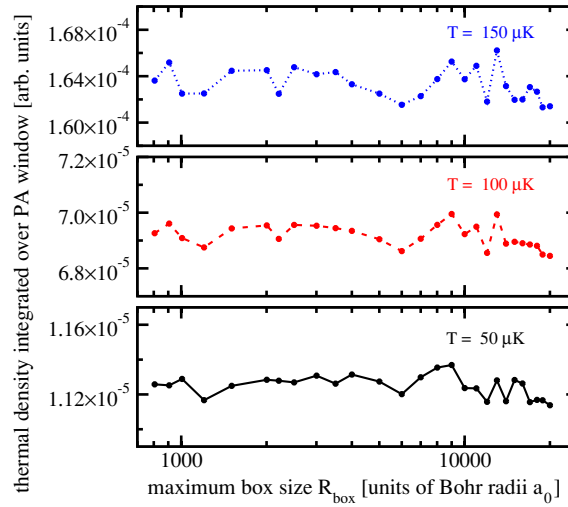


Figure 5. The unnormalized thermal density, $Z_{\text{eq,box}} \cdot \rho_{T,\text{box}}(R)$, integrated over the ‘photoassociation window’ as a function of the box size R_{box} for $T = 50 \mu\text{K}$ (black solid line), $T = 100 \mu\text{K}$ (red dashed line) and $T = 150 \mu\text{K}$ (blue dotted line). The number of grid points is $N_R = 1024$, R_{box} is varied by changing the grid mapping parameter β_{grid} . Shown are the values for two ^{87}Rb atoms interacting via the $X^1\Sigma_g^+$ ground state potential.

The correct treatment of higher l waves becomes even more important when shape resonances occur as in the example of ^{87}Rb . The contribution from the resonant l is then one to two orders of magnitude larger than for all other l , including the s -wave (in our calculations $l_{\text{res}} = 2$ for $^{87}\text{Rb}_2 X^1\Sigma_g^+$ as well as for $^{87}\text{Rb} a^3\Sigma_u^+$). This is explained by an increased probability density at intermediate range due to the shape resonance (cf figures 2(b), (e) for $^{87}\text{Rb}_2 X^1\Sigma_g^+$). A shape resonance in the scattering of two ^{87}Rb atoms colliding in the lowest triplet surface has been experimentally observed around $270 \mu\text{K}$ (Thomas *et al* 2004, Buggle *et al* 2004) and ascribed to the d -wave (Boesten H *et al* 1997).

4.4. Equivalence of averages on a finite-size grid and via box-independent continuum states

For short pulses and for detunings large enough such that the ‘photoassociation window’ is well defined, the final excited state population is proportional to the probability density in the ‘photoassociation window’. This is due to the fact that the ground state probability distribution is not equilibrated on the timescale of the pulse. The unnormalized thermal density integrated over the ‘photoassociation window’, $\int_{R_{\text{min}}}^{R_{\text{max}}} dR Z_{\text{eq,box}} \cdot \rho_{T,\text{box}}(R)$, shown in figure 5, is roughly independent of the box size R_{box} . The small fluctuations can be explained by the approximation introduced by the mapped grid method (Kokoouline *et al* 1999). The box size is varied by changing the parameter β_{grid} of the grid mapping while keeping the overall number of grid points constant, i.e. by stretching the variable grid step. The Fourier grid with constant grid step leads to an exponentially convergent representation of the Hamiltonian provided the number of grid points is large enough. This exponential convergence is lost with a semiclassical grid mapping (Kokoouline *et al* 1999, Willner *et al* 2004). However, much larger grid sizes which are essential to describe ultracold collisions become feasible.

Similarly the unnormalized photoassociation probability in the box (9) is independent of the box size for sufficiently large R_{box} which leads to a large value of the density of states $\frac{dn}{dE}$. For each l , the discrete summation over the discretized continuum states n can then be replaced

by an integral over energy $(2l+1) \int_0^\infty \frac{dn}{dE} e^{-\beta E} P_e^{El}(t_f) dE$. Following (8), $P_e^{El}(t_f)$ represents the population remaining on the excited state after the time propagation of the initial state φ_{nl} , i.e. the ground state eigenstate with energy $E = E_{nl}$ and angular momentum l normalized to unity in the box. By introducing the energy-normalized wavefunction $|E\rangle = 1/\sqrt{\frac{dE}{dn}} \varphi_{nl}$ (see section 2.2) the thermal average via box-independent ‘true’ continuum states is recovered. In this second approach one introduces the box-independent photoassociation probability density $\bar{P}_e^{El}(t_f)$ with dimension $1/E$ obtained by time propagating the energy-normalized initial state $|E\rangle$ and related to $P_e^{nl}(t_f)$ by $\bar{P}_e^{El}(t_f) = P_e^{El}(t_f) dn/dE$,

$$\begin{aligned} (2l+1) \sum_n e^{-\beta E_{nl}} P_e^{nl}(t_f) &\approx (2l+1) \int_0^\infty \frac{dn}{dE} e^{-\beta E} P_e^{El}(t_f) dE \\ &= (2l+1) \int_0^\infty e^{-\beta E} \bar{P}_e^{El}(t_f) dE. \end{aligned} \quad (18)$$

This explains the independence of the unnormalized photoassociation probability on the box size and demonstrates the equivalence of the two treatments using either box states or ‘true’ continuum provided R_{\max} is sufficiently large.

5. Approximation based on a scaling law

5.1. *s*-wavefunctions and quantum scaling law near a threshold

A further reduction of the numerical effort to estimate the total photoassociation probability per pulse can be achieved by considering the special properties of scattering states describing ultracold atoms. The required approximation is outlined below while the results obtained within this approximation are compared to those of the general procedure in section 6.2.

Some wavefunctions $|\varphi_n, l=0\rangle$ for *s*-wave stationary continuum states are represented in figure 6, for a pair of caesium atoms in the triplet state $a^3\Sigma_u^+(6S+6S)$. They are obtained by representing \hat{H}_g in a box of size $R_{\text{box}} = 19\,250a_0$ and subsequent diagonalization. For such a large box, the first continuum level with energy $\propto 1/R_{\text{box}}^2$ is found at 36.6 nK, so that the discretization of the continuum is correct for energies in the μK range. The wavefunctions $|E_{n,l=0}\rangle$, corresponding to the same energy but normalized per unit energy, are given by $|E_{n,l=0}\rangle = \left(\left[\frac{dE}{dn}\right]_{E_{ns}}\right)^{-1/2} |\varphi_n, l=0\rangle$, where for a box larger than the range of the potential V_g , the density of *s* states in the box is equal to

$$\left.\frac{dn}{dE}\right|_{E_{ns}} \sim \frac{R_{\text{box}}}{\pi\hbar} \sqrt{\frac{\mu}{2E_{ns}}}. \quad (19)$$

For the collisional wavefunctions, two different behaviours are observed depending on R , relative to a critical distance R_N which is the position of the last node of the last bound state for $l=0$. This node is common to all collisional wavefunctions in the relevant range of energies, respectively temperatures (cf figure 6(b)). As detailed by Crubellier and Luc-Koenig (2006), R_N can be calculated from reduced quantities,

$$R_N = X_N \sigma,$$

with $\sigma = [(2\mu C_6)/\hbar^2]^{1/4}$. X_N is obtained from $1/(2X_N^2) = \text{arccot}[(\eta - a_{\text{red}})/\eta] + 11/8\pi$ and $\eta = (2\pi)/[\Gamma(1/4)]^2 = 0.477\,989$, where $a_{\text{red}} = a/\sigma$ is determined by the scattering length a . For $R > R_N$ ($R_N = 82.3a_0$ for Cs_2 $a^3\Sigma_u^+(6S+6S)$), each continuum wavefunction with energy E_{ns} has its specific nodal structure determined by the local de Broglie wavelength $\lambda_{\text{dB}} = h/\sqrt{2\mu(E_{ns} - V_g(R))}$. At large distances, the wavefunctions $|\varphi_n, l=0\rangle$ have the same amplitude (cf figure 6(a)) which for a large box is approximately equal to $\sqrt{2/R_{\text{box}}}$ (the factor 1/2 accounting for the mean value of the oscillatory part).

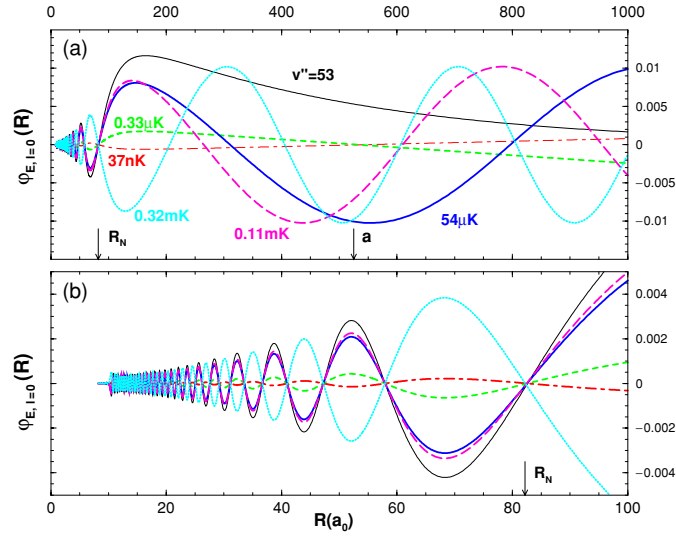


Figure 6. Wavefunctions for the stationary s -wave continuum states in the $\text{Cs}_2 a^3\Sigma_u^+(6S+6S)$ potential. (a) Long-range behaviour: same amplitude for all continuum wavefunctions. (b) Short-range behaviour: same nodal structure for all wavefunctions with R_N being the position of the last common node. The corresponding scattering energies $E_{ns} = k_B T$, calculated on a grid of length $19\,250a_0$, are 36.6 nK (red $-\cdot-$), 0.33 μK (green $---$), 54 μK (blue $---$), 0.11 mK (magenta $---$), 0.32 mK (cyan $\cdots\cdots$). The wavefunction for the last bound state $v'' = 53$ (divided by a factor of 5) is also displayed (thin black $---$). The value of the scattering length was taken to be $a = 538a_0$.

In contrast, for $R \leq R_N$, all continuum wavefunctions have the same nodal structure since the potential energy $\langle V_g(R) \rangle$ is larger than the kinetic energy $\langle \hat{T} \rangle$. These wavefunctions differ only by a short-range normalization factor, giving rise to scaling laws. The scaling factor $C(E_{ns})^{-1}$ can be derived by considering the behaviour near threshold in the simplest asymptotic model of a $-C_6/R^6$ potential with the short-range repulsive wall chosen to reproduce the scattering length (Crubellier and Luc-Koenig 2006). Near threshold, when the collision energy becomes smaller than the critical value $E_Q = 7^{7/2}2^4/3^6 \frac{\hbar^2}{2\mu\sigma^2} = 19.917\,53 \frac{\hbar^2}{2\mu\sigma^2}$, the quasi-classical Wigner–Kramers–Brillouin (WKB) approximation breaks down at intermediate distances around $R_Q \sim 3/(2^{1/2}7^{3/4})\sigma = 0.492\,297\sigma$, with $R_Q \sim R_N$, but remains valid both in the asymptotic region (where the potential is negligible), and at relatively short distances (where the local classical momentum $p(R) = 2\pi/\lambda_{\text{dB}}(R)$ is determined by the potential energy, and therefore stays independent of E). In this region, the energy-normalized radial wavefunction for an unbound state is written as

$$y(R) = \frac{1}{C(E)} \sqrt{\frac{2\mu}{\pi\hbar p(R)}} \cos\left(\left|\int_{R_o}^R p(R') dR'\right| - \frac{\pi}{2}\right), \quad (20)$$

where R_o is the turning point for the classical motion. The probability density at short range is completely determined by the energy-dependent factor $C^{-2}(E)$ which was introduced in the generalized form of multichannel quantum defect theory by Mies (1984) and Julienne and Mies (1989). This factor characterizes the departure from the WKB approximation at energies

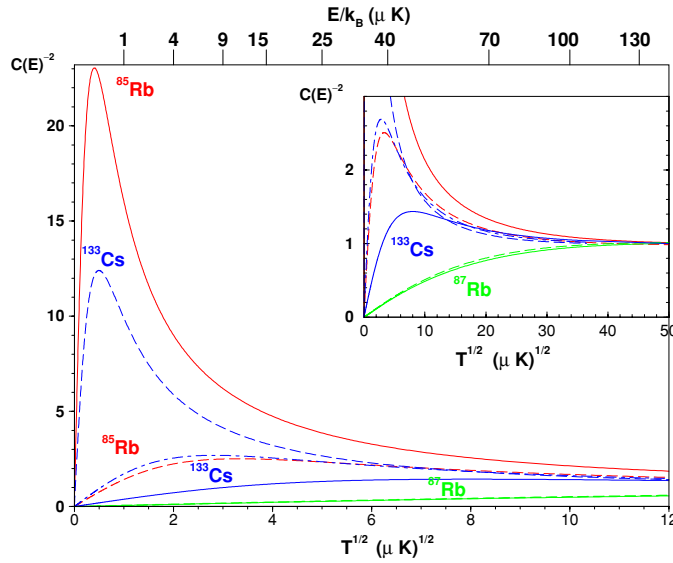


Figure 7. ‘Quantum suppression’: variation as a function of $\sqrt{E} \approx T^{1/2}$ of the density factor $C^{-2}(E)$ (21), which determines the short-range probability for s -wavefunctions (shown for $^{85}\text{Rb}_2$ (red), $^{87}\text{Rb}_2$ (green) and $^{133}\text{Cs}_2$ (blue)). In all cases, the WKB value $C(E) = 1$ is roughly reached at large energy $E/k_B > 50 \mu\text{K}$ and the Wigner threshold law ($C^{-2}(E) \propto \sqrt{E}$) is observed at a small energy. For sufficiently large $|a|$, a strong enhancement is observed in the probability density at short range. The values of the scattering length employed for collisions in singlet (—) and triplet (---) states are equal to, respectively, $3650a_0$ and $-332a_0$ for $^{85}\text{Rb}_2$ (Roberts *et al* 2001), $90.6a_0$ and $98.96a_0$ for $^{87}\text{Rb}_2$ (Marte *et al* 2002) and $280.37a_0$ and $2440a_0$ for $^{133}\text{Cs}_2$ (Chin *et al* 2004). The blue — · — line corresponds to $^{133}\text{Cs}_2$ with scattering length $538a_0$, the value used in the present time-dependent calculations.

close to threshold due to the large value of the de Broglie wavelength: $C(E) = 1$ if the WKB approximation is valid at all distances, and according to the Wigner threshold law for s -waves

$$C^{-2}(E) \propto \sqrt{E} \quad \text{for } E \rightarrow 0. \quad (21)$$

The rapid decrease of $C(E)$ with decreasing energy corresponds to the so-called ‘quantum suppression’ of cold collisions discussed by Côté *et al* (1996). Since the Wigner law is valid only very close to threshold and for a sufficiently large value of $|a|$, an enhancement of the probability density at short-range $C(E)^{-1} > 1$ is observed at low energy above threshold.

Near threshold, the variation of the ‘density factor’ is completely determined by the value of the reduced scattering length a_{red} . If $|a_{\text{red}}| > 0.5$, a resonance appears very close to threshold, as is seen from figure 8 in the systematic analysis by Crubellier and Luc-Koenig (2006). This resonance becomes sharper for larger values of $|a_{\text{red}}|$, especially for $a_{\text{red}} < 0$, and it generally occurs at energies in the micro-Kelvin range. The variation $C(E)^{-2}$, which represents the probability density at short range as a function of \sqrt{E} , is shown in figure 7 for singlet ground and lowest triplet state of $^{85}\text{Rb}_2$, $^{87}\text{Rb}_2$ and $^{133}\text{Cs}_2$. A strong resonant structure appears for the states $X^1\Sigma_g^+$ in $^{85}\text{Rb}_2$ and $a^3\Sigma_u^+$ in $^{133}\text{Cs}_2$, less pronounced structures for $a^3\Sigma_u^+$ in $^{85}\text{Rb}_2$ and $X^1\Sigma_g^+$ in $^{133}\text{Cs}_2$. For collisions in the ground singlet and triplet states of $^{87}\text{Rb}_2$, quantum suppression occurs below $50 \mu\text{K}$. A sharp resonance in $C(E)^{-2}$ is observed at an energy of $0.25 \mu\text{K}$ for the Cs_2 triplet state (cf figure 7), when the experimental value of the scattering length $a = 2440a_0$ obtained from precision Feshbach spectroscopy by

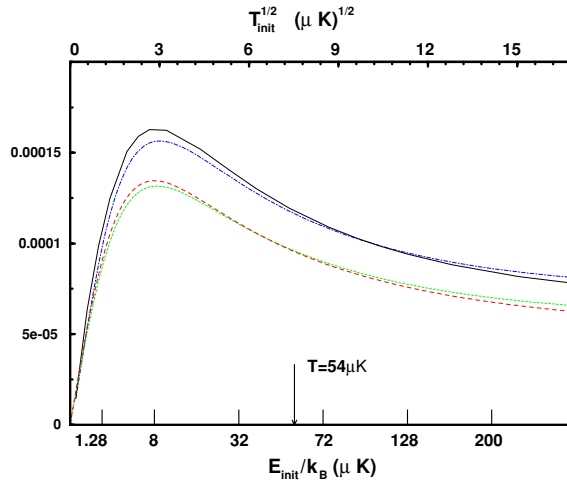


Figure 8. Scaling law for the photoassociation probability per pulse (black —), the Franck-Condon factor between the initial state and the resonantly populated vibrational state, (blue — · —), and the ground state probability density at the external Condon point R_L (green ---) [drawn in arbitrary units]; the ground state wave function is normalized per unit energy. The dimensionless short-range density factor $C(E)^{-2}$ (divided by the factor 210^4) is also reported (red ·····). Photoassociation to $\text{Cs}_2 0_g^-(6S+6P_{3/2})$ and a chirped laser pulse of duration $\tau_C = 36$ ps and chirp rate $\hbar\chi = -0.025 \text{ cm}^{-1} \text{ ps}^{-1}$ was assumed. The temperature $T = 54 \mu\text{K}$ of the atomic gas at thermal equilibrium is indicated by the arrow.

Chin *et al* (2004) is used to fit the potential (Crubellier and Luc-Koenig 2006). In contrast, when considering the $a^3\Sigma_u^+$ potential computed by Spiess (1989) which is used below in the time-dependent calculations, a smaller value $a = 538a_0$ for the scattering length is obtained. The energy variation of the short-range probability $C^{-2}(E)$ then manifests a less pronounced resonant structure at a higher energy ($8 \mu\text{K}$, see figure 7). This difference illustrates the high sensitivity of the resonance phenomenon, and hence of the photoassociation probability, to the value of the ground state scattering length.

5.2. Use of the scaling law near threshold: total s -wave photoassociation probability

The energy dependence of $C^{-2}(E)$ carries over to the energy dependence of the Franck-Condon factor $|\langle 1/\sqrt{dE_{n,l=0}/dn} \varphi_g | \varphi_e \rangle|^2$ (representing the overlap of the energy-normalized scattering wavefunctions $1/\sqrt{dE_{n,l=0}/dn} \varphi_g(R)$ with the short-range excited state vibrational wavefunction). It also determines the energy dependence of the s -wave photoassociation probability per pulse P_e^{Es} in the regime where photoassociation is governed by Franck-Condon factors, i.e. for weak fields or adiabatic population transfer, and with the laser detuning large enough such that $R_L \leq R_N$. This is illustrated in figure 8 where P_e^{Es} and $|\langle 1/\sqrt{dE_{n,l=0}/dn} \varphi_g | \varphi_e \rangle|^2$ are shown for the photoassociation of caesium to the $0_g^-(6S+6P_{3/2})$ state as a function of the relative kinetic energy E of the two atoms. The detuning of the pulse is fixed at $\Delta_L = 2.656 \text{ cm}^{-1}$ respective to the D_2 line where the central frequency is resonant with the $v = 98$ level in the external well of the $0_g^-(6S+6P_{3/2})$ potential. Also depicted is the probability density of the ground state wavefunction $|\varphi_g(R = R_L)|^2/(dE_{n,l=0}/dn)$ at the Condon point R_L which obeys a similar energy dependence, provided R_L is smaller or not much larger than R_N .

The knowledge of the energy dependence of $C^{-2}(E)$ can be used to markedly reduce the computational effort by avoiding time-dependent calculations for a large number of collision

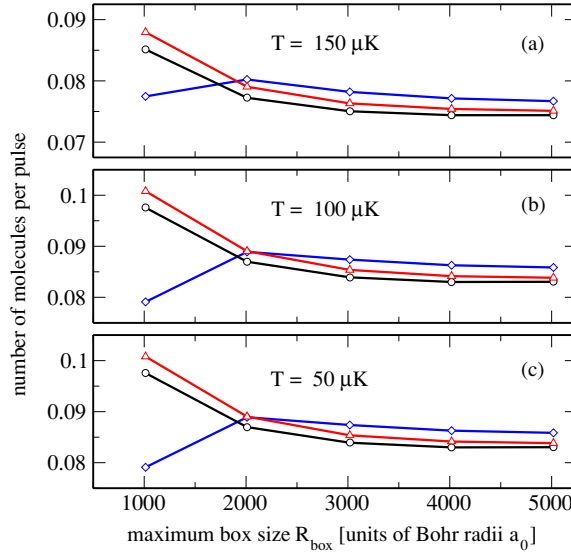


Figure 9. The number of excited state $\text{Cs}_2(0_g^-(P_{3/2}))$ molecules per pulse (4) as a function of the box size R_{box} for $T = 150 \mu\text{K}$ (a), $T = 100 \mu\text{K}$ (b), and $T = 50 \mu\text{K}$ (c) assuming the number of atoms to be $N = 10^7$ at a density $N/V = 10^{10} \text{ cm}^{-3}$ and neglecting excitation to other states. The atoms are supposed to be non-polarized with $f = 3$. $N_{\text{exc,tot}}^{\text{mol}}$ is obtained from $v_{\text{box}} \cdot \langle \hat{\mathbf{P}}_e \rangle_{T,\text{box}} / Z_{\text{eq,box}}$ (black circles), $v_{\text{box}} \cdot \langle \hat{\mathbf{P}}_e \rangle_{T,\text{box}} / Z_{\text{eq,box}}^{\text{free}}$ (red triangles), and from $v_{\text{box}} \cdot \langle \hat{\mathbf{P}}_e \rangle_{T,\text{box}} / Z_{\text{eq,box}}$ where $\langle \hat{\mathbf{P}}_e \rangle_{T,\text{box}}$ is calculated as an integral over energy-normalized states (blue squares). The sum in the numerator is evaluated up to $l = 11$ while l_{max} is used in the calculation of the partition function. The pulse is described in the text.

energies E . As illustrated in figure 8, it is sufficient to compute the probability for a single energy E_0 and to employ the scaling law,

$$\bar{P}_e^{Es} = \bar{P}_e^{E_0} \left[\frac{C(E)}{C(E_0)} \right]^{-2}, \quad (22)$$

to deduce the results for all energies in the threshold range. The total photoassociation probability per pulse is then given by integrating over E ,

$$P(T) = \frac{1}{Z_{\text{eq}}} \int e^{-\beta E} \bar{P}_e^{Es} dE, \quad (23)$$

where Z_{eq} and $Z_{\text{eq,box}} \frac{V}{v_{\text{box}}}$ are assumed to be identical. Total photoassociation probabilities obtained this way are presented in section 6.2.

6. Results: total photoassociation probability per pulse

6.1. Calculations in a 3D box

The total number of excited state molecules per pulse, calculated from (4) and (9), is shown in figure 9 for $\text{Cs}_2(0_g^-(P_{3/2}))$ and in figure 10 for $^{87}\text{Rb}_2(0_u^+(P_{1/2}))$. In both cases, the number of atoms is assumed to be $N = 10^7$ at a density $N/V = 10^{10} \text{ cm}^{-3}$ which corresponds to the Rb-MOT conditions of Salzmann *et al* (2006). The box volume is calculated as $v_{\text{box}} = 4\pi R_{\text{box}}^3/3$. The atoms are supposed to be non-polarized, and f is taken to be 3 (1) for ^{133}Cs (^{87}Rb). The pulse parameters are chosen as $\tau_L = 57.5 \text{ ps}$, $\tau_C = 110 \text{ ps}$ (i.e. $\hbar\chi = -0.002 \text{ cm}^{-1} \text{ ps}^{-1}$), $\Delta = 0.675 \text{ cm}^{-1}$ and pulse energy 19 nJ for caesium (pulse \mathcal{P}_-^{122} of Koch *et al* (2006a), and

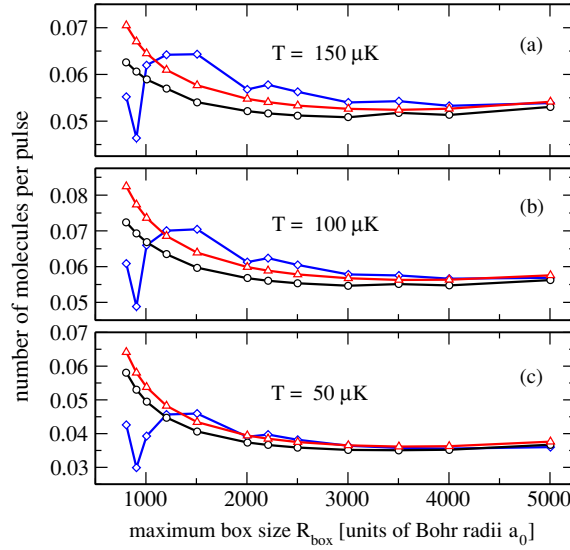


Figure 10. The number of excited state $\text{Rb}_2(0_u^+(P_{1/2}))$ molecules per pulse (4) as a function of the box size R_{box} for $T = 150 \mu\text{K}$ (a), $T = 100 \mu\text{K}$ (b), and $T = 50 \mu\text{K}$ (c) assuming the number of atoms to be $N = 10^7$ at a density $N/V = 10^{10} \text{ cm}^{-3}$ and neglecting excitation to the 1_g and 0_g^- excited states. The atoms are supposed to be non-polarized with $f = 1$. The meaning of the symbols is identical to that in figure 9. Both numerator and partition function are evaluated up to l_{max} . The pulse is described in the text.

$\tau_L = \tau_C = 10 \text{ ps}$ (i.e. $\chi = 0$), $\Delta = 4.1 \text{ cm}^{-1}$, $\mathcal{E} = 4.2 \text{ nJ}$ (cf Koch *et al* (2006b)) for rubidium. The pulse energy is estimated as $\mathcal{E} = \varepsilon_0 c \sqrt{\pi} \pi r_B^2 \mathcal{E}_0^2 \sqrt{\ln 2} \tau_L / 2$ with ε_0 the electric constant, c the speed of light, \mathcal{E}_0 the maximum amplitude of the pulse before chirping and r_B the radius of the laser beam ($r_B = 300 \mu\text{m}$ is assumed).

Three different ways to calculate $N_{\text{exc,tot}}^{\text{mol}}$ are compared: $\langle \hat{\mathbf{P}}_e \rangle_{T,\text{box}}$ is evaluated by summing over n and l in the numerator while employing the box partition function (black \circ) and the partition function of the free spherical waves (red \triangle) as well as by replacing the sum over n by $\int_0^\infty dE$ (18) while summing over *all* l and employing the box partition function (blue \square). It is clearly seen in figure 9 and figure 10 that the number of excited state molecules can be converged by increasing the size of the box. For caesium (rubidium), reliable results are obtained for $R_{\text{box}} \geq 4000a_0$ ($R_{\text{box}} \geq 3000a_0$). If R_{box} is too small, the density of states required for calculating the integral $\int_0^\infty dE$ which is approximated by the energy level difference $\Delta n / \Delta E_{nl}$ is not represented correctly. Therefore the three methods to evaluate $N_{\text{exc,tot}}^{\text{mol}}$ differ markedly for $R_{\text{box}} \leq 2000a_0$. The number of $\text{Cs}_2(0_g^-(P_{3/2}))$ molecules per pulse is estimated as 0.10 (0.16), 0.08 (0.13) and 0.07 (0.12) for 50 μK , 100 μK and 150 μK assuming non-polarized (polarized) atoms and $f = 3$. For $\text{Rb}_2(0_u^+(P_{1/2}))$ 0.04 (0.10), 0.06 (0.17), and 0.05 (0.15) are obtained for non-polarized (polarized) atoms, $f = 1$ and the respective temperatures. These values do not yet include the statistical factors $d_{2s+1\Sigma} / d_A^2$. A simple estimate of the molecule formation rate can be obtained by multiplying these numbers with the repetition rate of the laser. However, this assumes that each photoassociation pulse acts on an initial state in thermal equilibrium, i.e. the time between pulses is supposed to be long enough for the sample to equilibrate. Note that for $\text{Rb}_2(0_u^+(P_{1/2}))$ the photoassociation probability is higher for 100 μK and 150 μK than for 50 μK . This is due to the shape resonance for $l = 2$ (cf figure 2). A detailed investigation of this phenomenon is beyond the scope of this study and shall be given elsewhere.

6.2. Calculations using a scaling law: comparison to the 3D box calculations

If the calculations of section 6.1 are restricted to the s -wave, the validity of the discretization of the continuum (18) and of taking the analytical partition function Z_{eq} (12) and the box partition function $Z_{\text{eq,box}} \frac{V}{v_{\text{box}}}$ to be identical can be checked. Photoassociation of Cs_2 is considered for the same pulse conditions as in section 6.1, in particular with a detuning $\Delta = 0.675 \text{ cm}^{-1}$. The total probability per pulse is determined by solving the coupled equations (16) for a single energy $E_0 = k_B T_0$, $T_0 = 54 \text{ } \mu\text{K}$, and by integrating (23) for $50 \text{ } \mu\text{K}$, $100 \text{ } \mu\text{K}$ and $150 \text{ } \mu\text{K}$. Since the $a^3 \Sigma_u^+$ potential computed by Spiess which corresponds to a scattering length $a = 538a_0$ is employed, the energy variation of (22) corresponds to a broad resonance (cf section 5.1). The total probability per pulse is found to be 0.059, 0.033, and 0.023 for $50 \text{ } \mu\text{K}$, $100 \text{ } \mu\text{K}$ and $150 \text{ } \mu\text{K}$. According to the calculations of the previous section, the s -wave contributes respectively 63% (78%), 41% (53%) and 31% (38%) to the total photoassociation probability for non-polarized (polarized) atoms. This can be used to extrapolate the s -wave contributions of the present section to 0.094 (0.075), 0.08 (0.062) and 0.074 (0.061) molecules per pulse for non-polarized (polarized) atoms and the respective temperatures of $50 \text{ } \mu\text{K}$, $100 \text{ } \mu\text{K}$ and $150 \text{ } \mu\text{K}$. Comparing to the probabilities obtained with the full numerical averaging procedure of section 6.1, excellent agreement between the two methods is obtained emphasising the validity of the scaling law procedure.

In case of a potential corresponding to a larger value of the scattering length, $a = 2440a_0$ (Chin *et al* 2004), the scaling law yields a sharp resonance structure at $8 \text{ } \mu\text{K}$ (cf figure 7). The energy averaging then provides slightly different results for the photoassociation probability: at $T = 50 \text{ } \mu\text{K}$, $100 \text{ } \mu\text{K}$ and $150 \text{ } \mu\text{K}$, the integral $\int_0^\infty [C(E)]^{-2} e^{-\beta E} dE$ is larger by a factor of, respectively, 1.41, 1.24 and 1.17 for $a = 2440a_0$ compared to $a = 538a_0$. At lower temperatures, on the order of $8 \text{ } \mu\text{K}$ or below, a marked difference is observed, for example at $T = 1 \text{ } \mu\text{K}$ this factor is equal to 6.8. It should furthermore be noted that the temperature dependence of $P(T)$ differs markedly from the Wigner law, where for s -wave the threshold law $\bar{P}_c^{Es} \propto \sqrt{E}$ is associated with the variation $P(T) \propto T^{3/2}$. In the present calculation $P(T) \propto T^\alpha$ with $\alpha \sim 2/3$ for $a = 2440a_0$ and $\alpha \sim 4/5$ for $a = 538a_0$.

The present values for the total photoassociation probability per pulse have to be compared with the estimates given previously by Luc-Koenig *et al* (2004a, 2004b) for the same photoassociation reaction in a caesium MOT. In photoassociation at a larger detuning $\Delta_L = 2.656 \text{ cm}^{-1}$ with pulses $\tau_L = 15 \text{ ps}$, $\tau_C = 34.8 \text{ ps}$ and $\tau_L = 12 \text{ ps}$, $\tau_C = 46.6 \text{ ps}$, respectively, 0.69 and 1.40 molecules per pulse were found. This order of magnitude of one molecule per pulse is attributed to the different MOT conditions with $N = 10^8$ atoms in the same volume of $\sim 10^{-3} \text{ cm}^3$, i.e. a density of 10^{11} cm^{-3} as in the Orsay experiments described by Fioretti *et al* (1998). In such conditions, the pulse parameters considered here (with smaller detuning compared to Luc-Koenig *et al* (2004a)) would yield as much as 5.9 molecules per pulse formed from pairs of atoms colliding with s -wave scattering. When all the partial waves are considered, about 10 molecules per pulse are predicted.

7. Beyond the concept of a ‘photoassociation window’

The present paper has focussed on an excitation mechanism where population transfer from the ground to the excited state takes place within a ‘photoassociation window’. As discussed by Luc-Koenig *et al* (2004a, 2004b), other efficient mechanisms may exist such as non-adiabatic population transfer. Thus population in the excited state at large distances may be created which merely reflects the ground state wavefunction. Figure 11 compares two different excitation mechanisms: non-adiabatic population transfer leads to a wavepacket spreading

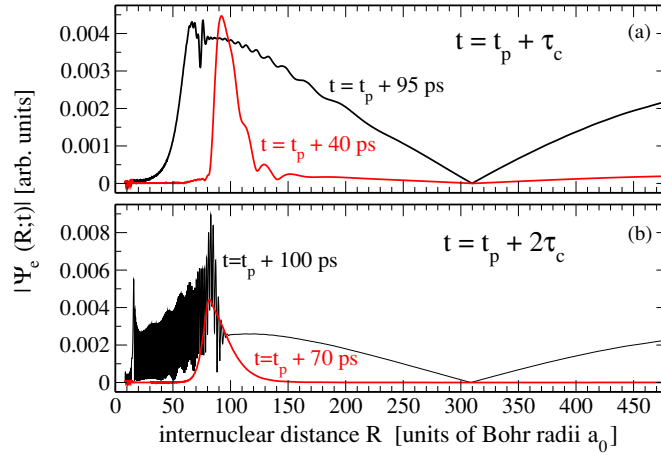


Figure 11. Two mechanisms of photoassociation: excited state wavepacket $|\Psi_{0_g^-}(R, t)|$ in the $\text{Cs}_2(0_g^-(P_{3/2}))$ state at the time $t = t_p + \tau_c$ (a) and $t = t_p + 2\tau_c$ (b) after the pulse maximum $t = t_p$. Two pulses with different spectral bandwidths are compared: $\hbar\delta\omega = 0.981 \text{ cm}^{-1}$ for $\tau_L = 15 \text{ ps}$, $\tau_C = 36 \text{ ps}$ (red curve) and $\hbar\delta\omega = 2.453 \text{ cm}^{-1}$ for $\tau_L = 6 \text{ ps}$, $\tau_C = 96 \text{ ps}$ (black curve). For small spectral bandwidth only adiabatic population transfer within the photoassociation window is observed (red curve), while for broad spectral bandwidth a non-adiabatic mechanism transfers population both at short and at long distances (black curve). At long distances the wavepacket is similar to the initial continuum wavefunction in the $a^3\Sigma_u^+$ state.

from large to small distances (black curve), while a very localized wavepacket within the photoassociation window is created by adiabatic population transfer (red curve). At the end of the pulse the wavepacket in the excited state can be written as

$$\bar{\Psi}_e(R, t_f) = \bar{\Psi}_e^{\text{win}}(R, t_f) + \alpha \bar{\Psi}_g(R, t_0), \quad (24)$$

i.e. as the sum of a wavepacket transferred in the ‘photoassociation window’ $\bar{\Psi}_e^{\text{win}}(R, t_f)$ and a long-range wavefunction proportional to the initial continuum wavefunction. As discussed by Luc-Koenig *et al* (2004b), the complex proportionality factor α is both R -independent and energy independent in the threshold region.

For the short-range contribution, which is obtained by subtracting $\alpha \bar{\Psi}_g(R, t_0)$ from the photoassociated wavepacket, the thermal average can be computed as described in the present paper, giving a lower limit to the number of photoassociated molecules. When the interference term between the two contributions can be neglected, the thermal average for the second term is trivial, since it reflects the thermal average of the initial distribution of atom pairs. However, the molecules formed in such a way may easily decay into pairs of hot atoms. The evaluation of the number of these photoassociated molecules is therefore of interest only, if efficient stabilization mechanisms can be found. This should be further developed in a forthcoming paper.

In situations where the long-range contribution dominates in (24), calculations with thermal Gaussian wavepackets as initial state should be justified. This again will be further developed in a forthcoming paper.

8. Conclusions

A general method to calculate the absolute number of molecules produced in a pulsed photoassociation scheme using a finite grid was derived. The absolute number of molecules

per pulse is calculated from the thermally averaged photoassociation probability which is determined by the pulse parameters and the initial pair density assumed to be in thermal equilibrium. The thermal average is obtained by decomposing the density operator into a sum of projections. This decomposition is not unique. Each projection is determined by a pure wavefunction for which the photoassociation probability can be calculated exactly. To keep the calculation feasible, the smallest possible number of projections should be used. The different physical limits lead to different projection schemes.

Approximations based on two limiting cases were discussed: (i) for $T \rightarrow 0$ photoassociation is dominated by s -wave collisions and the threshold laws determine the shape of the energy dependence of the initial s -wave density. Calculations for one energy of the colliding pair are sufficient, since results for the other energies can easily be deduced through a scaling law. (ii) When the potential energy of the initial states can be neglected relative to the kinetic energy which is true either for high temperatures or in the limit of zero detuning, i.e. photoassociation at extremely long range, then a decomposition of the density into thermal Gaussian wavepackets should be employed.

Even beyond these two limiting cases, a small grid and a small number of partial waves (typically on the order of 10) were shown to be sufficient to calculate the absolute number of molecules per pulse. For the case of s -wave scattering, the results of a single calculation with averaging via the scaling law and of the full numerical averaging procedure were compared, and good agreement was found. For the studied temperatures, between 50 μK and 150 μK , the photoassociation reaction is determined not only by s -wave collisions, and higher l -waves have to be considered. For typical MOT temperatures, a density of 10^{10} cm^{-3} and a detuning of about 4 cm^{-1} , the number of molecules per pulse in an order of magnitude estimate is obtained as 0.1 for $^{87}\text{Rb}_2(0_u^+(P_{1/2}))$. In the same conditions similar results should be obtained for caesium. However, when considering a typical caesium MOT with a density of 10^{11} cm^{-3} , the calculations predict formation of about $10^{133}\text{Cs}_2(0_g^-(P_{3/2}))$ molecules per pulse. Indeed, the pulse parameters and especially the detuning are better optimized than in previous calculations by Luc-Koenig *et al* (2004a, 2004b) where one molecule per pulse was predicted. In summary, the calculations imply a sufficient number of molecules to be detected for both rubidium and caesium assuming an experiment carried out at a repetition rate of 100 kHz which allows for equilibration between two photoassociation pulses.

These numbers should be considered as an order of magnitude estimate. Future work shall address the population of rotational levels in the excited state. Furthermore, for any specific experiment with given preparation of the atoms in hyperfine sublevels and polarization of the laser, the angular part of the transition dipole moment should be introduced properly.

The scaling law derived for s -wave scattering can with little effort be generalized to higher partial waves, leading to the determination of the partial density of probability at short range. This will allow us to compare the numerical averaging procedure to the method using threshold laws in the general case. It is expected that the number of photoassociated molecules can then be obtained with much less numerical effort by performing dynamical calculations for a single energy for each value of l and by employing generalized scaling laws.

Finally, the present work is restricted to the formation of molecules via adiabatic transfer within a ‘photoassociation window’. The efficiency of another mechanism, involving population transfer at large distances, should be explored in future work, in connection with the possibilities for stabilizing such molecules. Considering an initial thermal distribution of atoms, a different averaging procedure then should be implemented to describe this new mechanism.

Acknowledgments

We acknowledge fruitful discussions with Avinoam Ben-Shaul and Uli Poschinger. This work has been supported by the Deutsche Forschungsgemeinschaft (CPK) and the European Union in the frame of the Cold Molecule Research Training Network under contract HPRN-CT-2002-00290. EL-K, FM-S and AC belong to a team member of the Institut Francilien de Recherche des Atomes Froids. Three of us (FM-S, EL-K and RK) wish to acknowledge Esther, Iris and Peleg, respectively, for stimulating appearance during the writing of this paper.

References

- Boesten H M J M, Tsai C C, Gardner J R, Heinzen D J and Verhaar B J 1997 *Phys. Rev. A* **55** 636
- Brown B L, Dicks A J and Walmsley I A 2006 *Phys. Rev. Lett.* **96** 173002
- Buggle Ch, Léonard J, von Klitzing W and Walvaren J T M 2004 *Phys. Rev. Lett.* **93** 173201
- Chin C, Vuletić V, Kerman A J and Chu S 2004 *Phys. Rev. A* **70** 032701
- Comparat D, Drag C, Laburthe Tolra B, Fioretti A, Pillet P, Crubellier A, Dulieu O and Masnou-Seeuws F 2000 *Eur. Phys. J. D* **11** 59
- Côté R, Heller E J and Dalgarno A 1996 *Phys. Rev. A* **53** 234
- Crubellier A and Luc-Koenig E 2006 *J. Phys. B: At. Mol. Opt. Phys.* **39** 1417
- Dalibard J, Castin Y and Mølmer K 1992 *Phys. Rev. Lett.* **68** 580–3
- Doyle J, Friedrich B, Krems R V and Masnou-Seeuws F 2004 *Eur. Phys. J. D* **31** 149–64
- Fioretti A, Comparat D, Crubellier A, Dulieu O, Masnou-Seeuws F and Pillet P 1998 *Phys. Rev. Lett.* **80** 4402–5
- Friedrich H 1998 *Theoretical Atomic Physics* (Berlin: Springer)
- Gelman D and Kosloff R 2003 *Chem. Phys. Lett.* **381** 129–38
- Hill T L 1960 *An Introduction to Statistical Thermodynamics* (Reading, MA: Addison-Wesley)
- Julienne P S 1996 *J. Res. Natl. Inst. Stand. Technol.* **101** 487
- Julienne P S and Mies F H 1989 *J. Opt. Soc. Am. B* **6** 2257
- Julienne P S, Smith A M and Burnett K 1993 *Adv. At. Mol. Opt. Phys.* **30** 141
- Koch C P, Luc-Koenig E and Masnou-Seeuws F 2006 *Phys. Rev. A* **73** 033408
- Koch C P, Kosloff R and Masnou-Seeuws F 2006 *Phys. Rev. A* **73** 043409
- Kokoouline V, Dulieu O, Kosloff R and Masnou-Seeuws F 1999 *J. Chem. Phys.* **110** 9865
- Kosloff R 1994 *Annu. Rev. Phys. Chem.* **45** 145–78
- Luc-Koenig E, Kosloff R, Masnou-Seeuws F and Vatasescu M 2004 *Phys. Rev. A* **70** 033414
- Luc-Koenig E, Masnou-Seeuws F and Vatasescu M 2004 *Eur. Phys. J. D* **31** 239–62
- Machholm M, Giusti-Suzor A and Mies F 1994 *Phys. Rev. A* **50** 5025
- Marte A, Volz T, Schuster J, Dürr S, Rempe G, van Kempen E G M and Verhaar B J 2002 *Phys. Rev. Lett.* **89** 283202
- Masnou-Seeuws F and Pillet P 2001 *Adv. At. Mol. Opt. Phys.* **47** 53–127
- Mies F H 1984 *J. Chem. Phys.* **80** 2514
- Roberts J L, Burke J P Jr, Claussen N R, Cornish S L, Donley E A and Wieman C 2001 *Phys. Rev. A* **64** 024702
- Salzmann W *et al* 2006 *Phys. Rev. A* **73** 023414
- Spiess N 1989 *PhD Thesis* Fachbereich Chemie, Universität Kaiserslautern
- Thomas N R, Kjaergaard N, Julienne P S and Wilson A C 2004 *Phys. Rev. Lett.* **93** 173202
- Vala J, Dulieu O, Masnou-Seeuws F, Pillet P and Kosloff R 2000 *Phys. Rev. A* **63** 013412
- Vardi A, Abrashkevich D, Frishman E and Shapiro M 1997 *J. Chem. Phys.* **107** 6166–74
- Vrahatis M N, Ragos O, Skiniotis T, Zafiroopoulos F A and Grapsa T N 1995 *Comput. Phys. Commun.* **92** 252
- Weiner J, Bagnato V S, Zilio S and Julienne P S 1999 *Rev. Mod. Phys.* **71** 1–85
- Willner K, Dulieu O and Masnou-Seeuws F 2004 *J. Chem. Phys.* **120** 548